A complexity science study: effect of critical current density on semiconductor laser diodes and integrated circuits

Jack Jia-Sheng HUANG
Department of Optoelectronics R&D, Source Photonics,
8521 Fallbrook Avenue, Suite 200, West Hills, CA 91304, USA

and

Yu-Heng JAN
Department of Optoelectronics R&D, Source Photonics,
No.46, Park Avenue 2nd Rd., Science-Based Industrial Park, Hsinchu, Taiwan

ABSTRACT

Complexity science is becoming increasingly poplular in order to more effectively tackle with the convoluted and multi-dimentional problems. In this work, we discuss the application of complexity science based on the case study of reliability physics of semiconductor laser diodes (LDs) and integrated circuits (ICs). We show the common effect of critical current density on laser diode and IC interconnect, and discuss its implication in device design. Our study also demonstrates that universal law of complexity science could be applied to seemingly different fields as the innovative, inter-disciplinary approach to resolve the ever-increasing complex problems.

Keywords: Complexity science, critical current density, semiconductor laser diode, integrated circuits, reliability, laser degradation, electromigration

1. INTRODUCTION

Complexity science is concerned with complex systems and problems that are dynamic, unpredictable and multi-dimensional, consisting of a collection of interconnected relationships and parts. [1,2]. As an emerging approach to research, complexity science is a study of a complex system based on a collection of theories and conceptual tools from an array of disciplines. For example, complexity science has been taken up in both mathematics and social sciences, and has become increasingly popular in health care [3,4] and semiconductor technology [5,6], as illustrated in Fig.1.

For semiconductor technology, electronic IC and photonic industries are starting to interact and collaborate together using multi-disciplinary approach in recent years, as shown in Fig.2 [6-9]. For example, the recent IC development started to incorporate more-than-Moore where the traditional digital chips incorporated the other functionalities such as analog/radio frequency (RF), Microelectromechanical systems (MEMS) and optical devices [10,11]. On the other hand, the photonic devices are starting to integrate Si photonics into design to enhance the performance and reduce the cost [12,13].

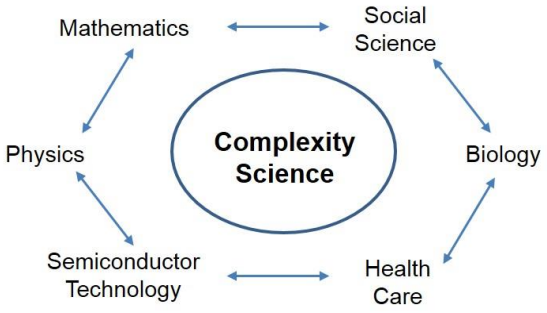

Figure 1. Schematic of complexity science and its applications in different fields.

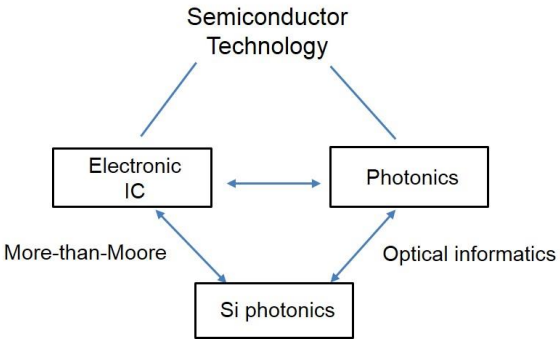

Figure 2. Schematic of interactions between the electronic IC and photonics within the semiconductor technology field. The IC and photonics are interacting with each other by means of more-than-Moore and optical informatics.

In the area of photonics, optical informatics has recently been identified as the dominant field of research to study optical technologies of transmitting, receiving, processing, storing and displaying [14]. Some of the universities such as National Research University (St. Petersburg, Russia), Warsaw University of Technology (Warsaw, Poland) and University of Rochester (Rochester, USA) are offering the optical informatics program in graduate school [6,8,9].

In our previous studies, we demonstrated the resemblence and analogy between IC and photonics [7]. We also showed the existence of critical current density in laser diodes [15]. In this paper, we study the similarity of critical current density in the laser diode and IC interconnect. We discuss the common effect of critical current density on device degradation and its implication in reliability extrapolation and design.

2. EXPERIMENT

2.1 Laser diode fabrication

Figure 3(a) shows the schematic of a laser diode (LD) where the current bias is applied to the top metal contact to generate the optical output power. Figure 3(b) shows the typical light vs. current (LI) curve of the LD. There is a transition point on the LI defined as the threshold current (I_{th}) below which the spontaneous emission occurs. Above the I_{th}, the power increases with the increasing current due to the stimulated emission [16].

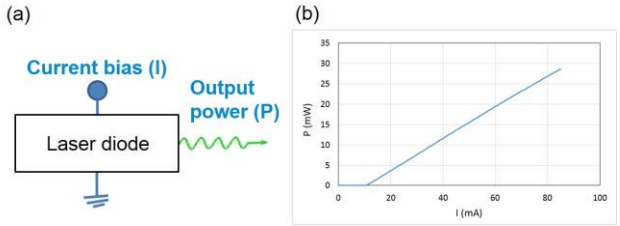

Figure 3. Schematics of (a) a laser diode and (b) its LI curve.

Several device structures have been employed to enhance the lasing efficiency, as shown in Fig.4. The laser structures were grown by the metal organic chemical vapor deposition (MOCVD) technique. The single-mode distributed feedback (DFB) was defined by holographic grating. For the ridge waveguide (RWG) structure in Fig.4a, one step regrowth after grating was performed to form the p-InP cladding and p^+-InGaAs contact. The active region consisted of InGaAlAs multi-quantum well (MQW) materials [17]. For the electro-absorption modulated laser (EML) in Fig.4b, the laser section was fabricated by the similar method as the RWG laser and integrated with the electro-absorption modulator (EAM) section in the front. The two sections were formed by butt-joint regrowth [18]. For the buried heterostructure (BH) structure in Fig.4c, three regrowth steps including grating overgrowth, blocking regrowth and final regrowth were performed to complete the epitaxial layers. The first regrowth was performed after the grating etch; the second regrowth was performed after the mesa etch to form the BH structure; the final regrowth consisted of the p-InP cladding and p^+-InGaAs contact [19].

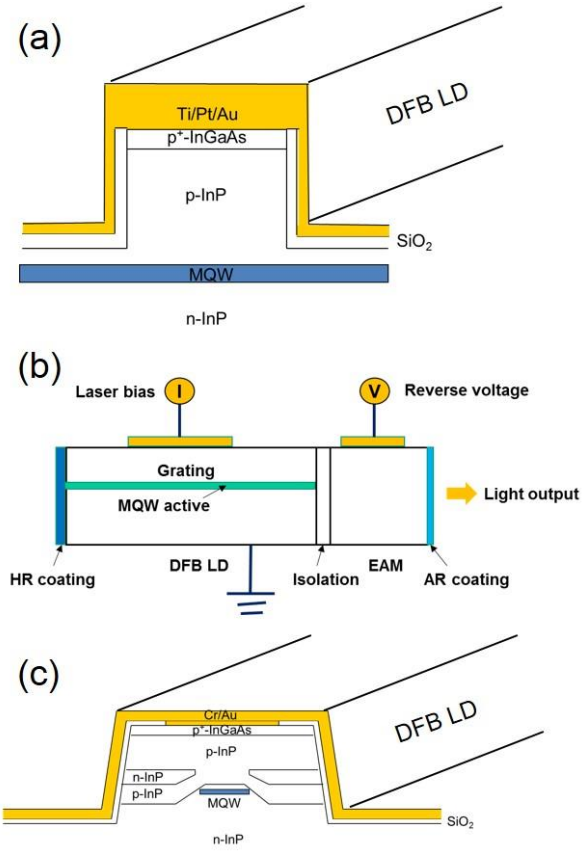

Figure 4. Schematics of different laser diode structures of (a) RWG (b) EML and (c) BH lasers.

The lasers were stressed with constant current densities. For simplicity, the current density (j) times the active width (w) was used as the measure of stress current intensity since the major variation was determined by the cavity length where the active width was fixed at 1.8μm. The stress current density times the width (j·w) or the stress current (I) divided by the cavity length (L) was ranging from 0.38 to 0.71 mA/μm to determine the critical current density.

2.2 IC interconnect sample preparation

The modern IC includes billions of transistors and interconnects. In order to ensure overall IC robustness, each transistor or interconnect needs to be highly reliable. To study the reliability of the transistor or interconnect, a dedicated test structure is usually used. Figure 5(a) shows an example of the via chain test structure to characterize

the electromigration of lower- and upper-level metal lines [20]. Figure 5(b) shows the resistance change as a function of aging time as a result of electromigration. The resistance of the metal conductor increases with time due to the void formation at the cathode.

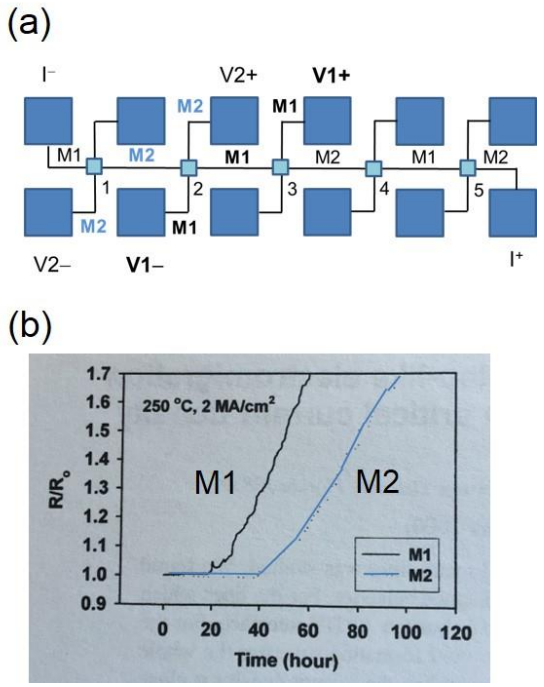

Figure 5. (a) Schematic of an IC via chain test structure and (b) example of electromigration-induced resistance change due to void formation.

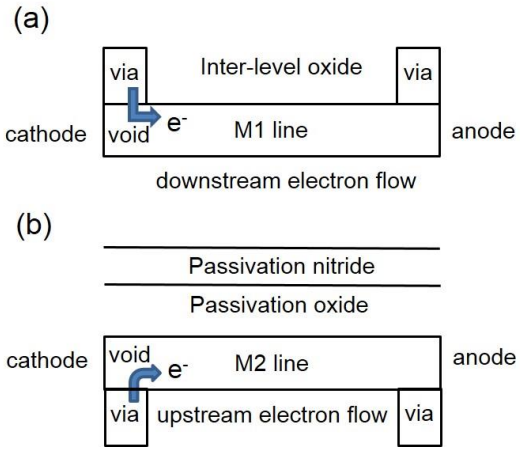

Figure 6. Schematic of IC interconnect and aging stress methodology.

The IC interconnect test structure included the lower-level metal (M1) line and upper-level metal (M2) line as shown in Fig.6 [20,21]. The M1 and M2 lines were electrically connected by the tungsten (W) via. The metal lines consisted of 30nm Ti/60nm TiN/450nm AlCu/25nm TiN stacks with length of 240μm and width of 0.36μm. The metal test structures were built on top of the high density plasma (HDP) oxide/Si substrate. The via was filled by chemical vapor deposition (CVD) W with 20nm Ti/50nm TiN coating barrier. The M2 line was passivated with HDP oxide and silicon nitride, and the planarization was achieved by chemical mechanical polishing (CMP) process.

The metal line structures were stressed with constant current densities ranging from 0.5 to 2 MA/cm^2 at 250°C. The resistance variations of M1 and M2 lines were a result of metal depletion or voiding at the cathode due to electromigration. The failure criterion for M1 and M2 were defined as the resistance increases of 20% and 4.5%, respectively to account for the sheet resistance effect [20,21].

3. RESULTS and DISCUSSIONS

3.1 Laser diode

In our previous defect diffusion model [15], it was assumed that the laser degradation was related to the diffusion from the defect source to the active region. The defect source included p-contact, BH interface or substrate dislocation network [19,22]. The flux of the defect diffusion can be expressed in Equation (1).

$$J = C\frac{D}{kT}(Q^*\rho j - \frac{\partial \mu}{\partial x}) \qquad \text{Eq. (1)}$$

where C is the atomic defect concentration, D is the diffusivity of the defect, k is the Boltzmann constant, and T is the temperature. The first term corresponds to the driving force from electrical current and field where Q* is the effective defect charge, ρ is the resistivity and j is the current density. The second term stands for the "backflow" force where μ is the chemical potential of the defect and x is the axis along the defect propagation direction.

When the backflow and the electrical force reach the equilibrium, the two forces cancel each other. At the equilibrium state, there is no net flux of defect diffusion. Hence, the threshold current (I_{th}) of the laser diode remains the same with no further increase. The critical current density can be related to the chemical potential in Equation (2).

$$Q^*\rho j_c = \frac{\Delta \mu}{l} \qquad \text{Eq. (2)}$$

where j_c is the critical current density where no laser degradation occurs, Δμ is the maximum chemical potential that the defect can build up locally, and l is the defect diffusion distance. The flux of defect can be rewritten in terms of critical current density

$$J = C\frac{D}{kT}Q^*\rho(j - j_c) \qquad \text{Eq. (3)}$$

The flux of defect can be simplified as the drift velocity according to the relation of v_d=J/C.

$$v_d = \frac{D}{kT}Q^*\rho(j - j_c) \qquad \text{Eq. (4)}$$

The failure time is proportional to the time to accumulate enough defects in the active region to cause the failure. The failure time can be expressed as

$$t_f = \frac{V_c}{Av_d} \qquad \text{Eq. (5)}$$

where V_c is the volume of defect needed to cause failure, and A is the top-view area of the laser stripe subjected to current injection. For laser diode, the area A is determined by the active width (w) and cavity length (L) as shown in Equation (6).

$$A = wL \qquad \text{Eq. (6)}$$

To compare Equation (5) with the experimental data that is more easily measured, the failure time t_f can be expressed in terms of j·w, as shown in Equation (7). The width of the active region is typically pre-determined by the process to match the performance design target. The typical active width is around 1.8μm for the laser diode.

$$t_f = \frac{(V_c / L)kT}{DQ^*\rho(j - j_c)w} \qquad \text{Eq. (7)}$$

By rearrangement of the variables, Equation (7) can be rewritten as Equations (8) where the first term corresponds to the intercept j_c·w, and the second term is for the slope of the variable t_f.

$$jw = j_c w + \frac{(V_c / L)kT}{DQ^*\rho}\left(\frac{1}{t_f}\right) \qquad \text{Eq. (8)}$$

In the experimental data, one common way to represent the statistical population of the wafer or group is by taking the 50% cumulative failure probability. For the failure time, the mean-time-to-failure (MTTF) is typically used to represent the 50% of the failure times taken from the lognormal distribution.

$$jw = j_c w + \frac{(V_c / L)kT}{DQ^*\rho}\left(\frac{1}{MTTF}\right) \qquad \text{Eq. (9)}$$

3.1.1. Critical current density of laser diodes

Figure 7 shows the plot of j·w vs. 1/MTTF to determine the j_c in Equation (9). Several interesting features were experimentally observed. First, there existed a critical current density, j_c, for all three types of lasers. Second, the value of j_c for the RWG was higher than those for the EML and BH types. The j_c value of RWG was 0.48 mA/μm, while the j_c values for EML and BH were 0.38 and 0.35 mA/μm, respectively. The lower j_c in the EML and BH types might be attributed to the regrowth. For the EML, there was butt-joint regrowth between the LD and EAM sections. For the BH, the mesa etch interface involved with regrowth [22].

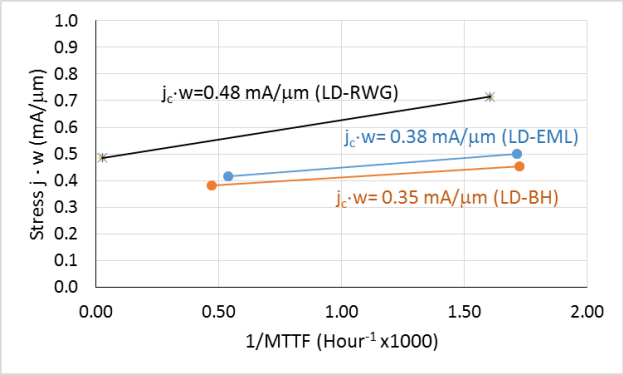

Figure 7. The plot of stress current density times active width versus reciprocal of MTTF for laser diodes. The critical current density is extracted from the intercept where 1/MTTF equals to zero.

3.1.2. Failure distributions of laser diode

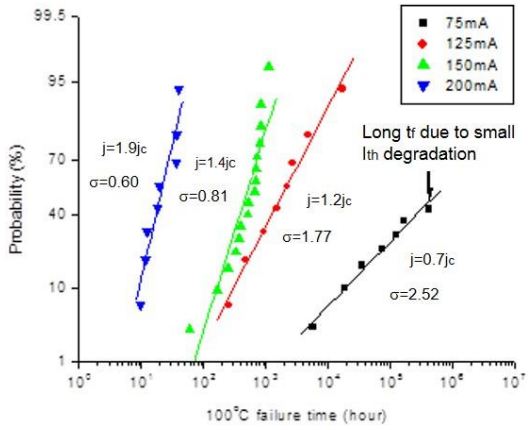

Figure 8. Failure time distributions of laser diodes subjected to different stress current density with respect to j_c. The symbols are the experimental data, and the lines are from regression fitting.

Figure 8 shows the failure time distributions of laser diodes as a function of stress current. In this case, the EML devices were subjected to different j. The failure distribution for each stress current was also denoted as the ratio of j/j_c. We noted that the failure times for the low stress current were typically longer than those for the high stress current. At the meantime, the sigma (σ) of the

failure times for the low stress current also tended to increase. In this case, σ increased from 0.60 to 2.52 when j was reduced from $1.9j_c$ to $0.7j_c$. The deviation of the failure distribution of the low stress regime from lognormal could be attributed to the effect of j_c. According to Equation (7), t_f was inversely proportional to $j-j_c$. The Monte-Carlo simulation would result in strong deviation of failure distributions as j approached j_c [23]. This was likely due to the smaller value of $(j-j_c)$ in the denominator.

3.2 IC interconnect

For IC interconnect, Blech and Herring reported a critical current density of electromigration below which no electromigration occurred [24,25]. The j_c of IC interconnect resulted from the back stress (σ) generated in the metal stripe as shown in Equation (10) where Z*e is the effective charge for electromigration, Ω is the atomic volume of the diffusing species, and $\partial\sigma/\partial x$ is the stress gradient in the metal conductor.

$$J = C\frac{D}{kT}(Z^*e\rho j - \Omega\frac{\partial\sigma}{\partial x}) \qquad \text{Eq. (10)}$$

The effect of critical current density on electromigration has been observed in Al, Al(Cu) and Cu dual-damascene vias [26-29]. Recently, Oates from TSMC [30] demonstrated similar deviation of failure time distributions from lognormal in the Cu dual-damascene as j approached j_c as predicted by Equations (11) and (12) where A_s is the cross-sectional area of the metal line defined by the width and thickness.

$$t_f = \frac{(V_c/A_s)kT}{DZ^*e\rho(j-j_c)} \qquad \text{Eq. (11)}$$

$$j = j_c + \frac{(V_c/A_s)kT}{DZ^*e\rho}(\frac{1}{t_f}) \qquad \text{Eq. (12)}$$

Equation (12) can again be represented in statistical expression shown in Equation (13) where MTTF is the 50% of the failure times from the cumulative probability.

$$j = j_c + \frac{(V_c/A_s)kT}{DZ^*e\rho}(\frac{1}{MTTF}) \qquad \text{Eq. (13)}$$

3.2.1. Critical current density of IC interconnect

Figure 9 plots j as a function of 1/MTTF for M1 and M2 lines. The critical current densities determined by the intercepts of j extending from the fitting lines were 0.34 and 0.61 MA/cm^2 for M1 and M2, respectively. The larger j_c of M2 was likely due to the SiN_x passivation that provided greater mechanical confinement due to the higher Young's modulus [20,31].

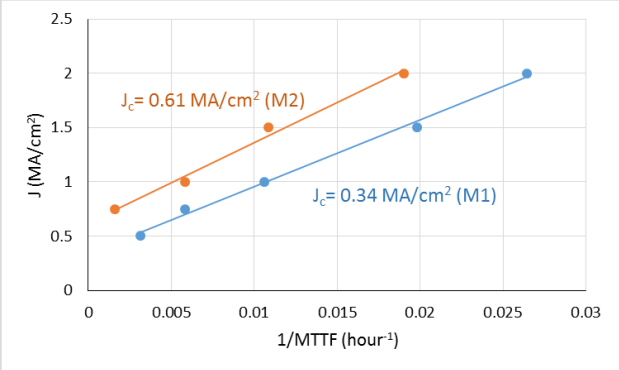

Figure 9. The plot of stress current density versus reciprocal of MTTF for IC interconnect where M1 is the lower-level metal line with downstream electromigration and M2 is the upper metal line with upstream electron flow. The critical current density is extracted from the intercept where 1/MTTF equals to zero.

3.2.2. Failure distributions of IC interconnect

Figure 10 shows the failure distributions of M2 line as a function of current density. The form of the failure distribution changed as j approached j_c. For current density well above j_c, the distributions were lognormal. For the devices subjected to j that was close to j_c, the failure distributions started to show deviation from the lognormal. For examples, the distributions of $j=1.1j_c$ and $j=0.8j_c$ in Fig.8 showed pronounced deviations with larger sigma.

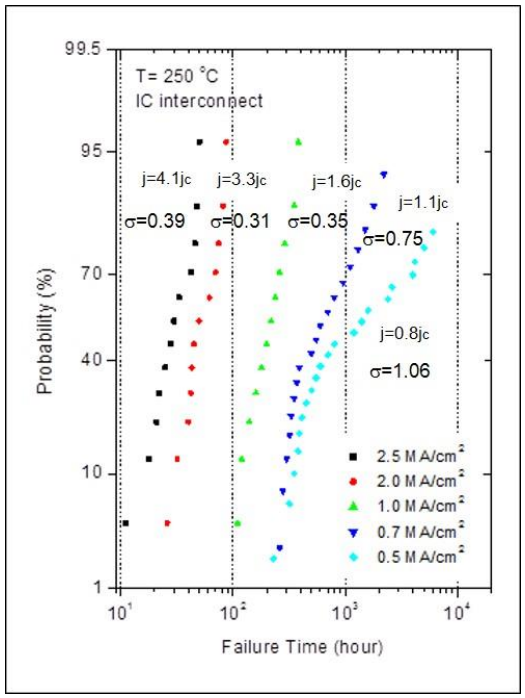

Figure 10. Failure time distributions of IC interconnect subjected to different stress current density. The symbols are the experimental data taken from the Au(Cu) metal line with W-plug via.

The other interesting finding was the universal behavior in the change of failure distribution as a function of j [23,29,30]. Based on the parameters of Equation (12), the sigma can be statistically expressed in Equation (14) where σ is the total sigma of the distribution, σ_{As} is the sigma related to the cross-sectional area of the metal line, and σ_T is the sigma related to temperature, and σ_0 is the sigma related to all other parameters. The second term relates to the statistical variation associated with cross-sectional area (A_s). The third term stands for the statistical variation from the temperature where E_a is the activation energy.

$$\sigma^2 = \sigma_0^2 + \frac{(j^2/A_s^2)}{(j-j_c)^2}\sigma_{As}^2 + (\frac{E_a}{kT})^2\sigma_T^2 \qquad \text{Eq. (14)}$$

The change in statistics is a fundamental property of contact/via electromigration and does not depend upon the contact or via structure or the metallization composition/structure.

3.3 Design implication

Comparison of failure distributions as a function of stress current density in the photonic laser diode and electronic IC interconnect showed striking similarity, as summarized in Table 1. Despite the seemingly different device structure and physics, both laser diode and IC interconnect showed strong dependence of failure distribution form as a function of critical current density. In both cases, the model predicted a force of backflow to offset the electrical driving force. The model also predicted a deviation from lognormal distribution with larger sigma when j was decreased to the vicinity of j_c.

Table 1. Physics and mathematical formulation of critical current density for photonic laser diode and electronic IC interconnect.

	Laser diode	IC interconnect
Model-diffusion flux	$J = C\frac{D}{kT}(Q^*\rho j - \frac{\partial\mu}{\partial x})$	$J = C\frac{D}{kT}(Z^*e\rho j - \Omega\frac{\partial\sigma}{\partial x})$
Model- jc	$jw = j_c w + \frac{(V_c/L)kT}{DQ^*\rho}(\frac{1}{t_f})$	$j = j_c + \frac{(V_c/A_s)kT}{DZ^*e\rho}(\frac{1}{t_f})$
Experimental results	$\sigma\uparrow$ as $j\rightarrow j_c$	$\sigma\uparrow$ as $j\rightarrow j_c$

In the following, we discuss the failure distribution and extrapolation for the high and low stress current regimes.

3.3.1. High stress regime ($j >> j_c$)

At the high stress regime, the failure distribution typically follows lognormal distribution since j is distantly away from j_c ($j >> j_c$). The benefit of applying the high stress regime includes the short stress time and the easy assessment of the failure rate. When the failure distribution follows lognormal, the failure in time (FIT) rate of a device can be estimated with good confidence and accuracy. The extrapolation based on the whole distribution or the low percentile is also expected to be consistent. Table 2 summarizes the various reliability aspects of high and low stress regimes.

Table 2. Effect of critical current density on photonic laser diode and electronic IC interconnect.

	High stress regime ($j >> j_c$)	Low stress regime ($j \rightarrow j_c$)
Failure distribution	Lognormal	Deviation from lognormal
Failure time	t_f is shorter	t_f is longer
Sigma	σ is smaller	σ is larger
FIT rate	Consistent from all parts of failure distribution	Varies depending upon whether the whole distribution or low percentile
Reliability assessment	Easy as long as not overstressed	Care needs to be taken for extrapolation

3.3.2. Low stress regime ($j \rightarrow j_c$)

Due to the effect of j_c, the t_f becomes significantly larger when j approaches j_c. At the meantime, the sigma of the failure distribution also increases with decreasing j. The deviation from lognormal distribution often requires careful assessment when performing the reliability extrapolation. While the larger t_f can improve the overall failure rate, the larger σ would also degrade the FIT rate to offset the benefit from larger t_f. Therefore, care needs to be taken when performing reliability extrapolation on the non-lognormal failure distribution at the low stress regime.

4. CONCLUSIONS

We have presented a case study of complexity science for the application of semiconductor technology. We have shown the common effect of critical current density in both photonic laser diode and electronic IC. The kinetics diffusion model predicted the existence of critical current density. The j_c showed universal effect on the form of failure distribution.

For the high stress regime ($j>>j_c$), the failure distribution showed lognormal. The reliability extrapolation was expected to be consistent from all parts of the failure distribution. The confidence of the reliability assessment in the normal/high stress regime was typically high as long as the devices were not overstressed to induce unwanted failure mechanism. As the j approached j_c in the low stress regime, the failure distribution showed deviation from lognormal with larger sigma. In the low stress regime, care needed to be taken when performing reliability extrapolation in order to achieve accurate estimate of FIT rate.

In this case study, we have demonstrated the feasibility of conducting multi-disciplinary approach to address the complex problems in the field of semiconductor technology. The promising example of photonic and electronic IC synergy could be applied to other fields of complexity science to create innovative approach based on a collection of theories and conceptual tools.

5. ACKNOWLEDGMENT

The authors wish to thank Jesse Chang for the assitance in test data collection, Source Photonics-Taiwan wafer fab for chip processing and testing, and Emin Chou for support of this work.

6. REFERENCES

[1] A. Miles, "Complexity in Medicine and Healthcare: People and Systems, Theroy and Practice", **J. Evaluation Clinical Practice**, Vol. 15, 2009, pp. 409-410.

[2] J. Ross and A.P. Arkin, "Complex Systems: from Chemistry to Systems Biology", **Proceed. National Academy Sciences**, Vol. 106, No. 16, 2009, pp. 6433-6434.

[3] M. Benham-Hutchins and T.D. Clancy, "Social Networks as Embedded Complex Adaptive Systems", **J. Nurs. Admin.**, Vol. 40, No. 9, 2010, pp. 352-356.

[4] J. Paley and E. Gail, "Complexity Theory as an Approach to Explanation in Healthcare: a Critical Discussion", **Int. J. Nurs. Study**, Vol. 48, No. 2, 2011, pp. 269-279.

[5] S.A. Kozlov, **Fundamentals of Femtosecond Optics**, Cambridge, UK: Woodhead Publishing, 2013.

[6] S.A. Kozlov, "Photonics and Optical Informatics", **National Research University of ITMO website**, St. Petersburg, Russia.

[7] J.S. Huang and Y.H. Jan, "Interconnected Analogy and Resemblence: from Classical Music to Modern Semiconductor Technology", **Int. J. Electrical Electronics Engineering**, Vol. 5, No. 2, 2016, pp. 1-8.

[8] **The Laboratory of Optical Informatics**, Center for Advanced Studies, Warsaw U. Tech. website, 2013.

[9] "Optics, Photonics and Optoinformatics", **U. Rochester** website.

[10] W. Arden, M. Brillouet, P. Cogez, M. Graef, B. Huizing and R. Mahnkopf, **"More-than-Moore" White Paper**, 2014.

[11] G.Q. Zhang and A.J. van Roosmalen, Ed. **More than Moore: Creating High Value Micro/Nanoelectronics Systems**, New York, NY: Springer, 2009.

[12] L. Fulbert, "Helios Brings Silicon Photonics Fabrication to EU Companies", **EUROPhotonics Magazines**, 2012.

[13] L. Vivien, J. Osmond, D. Marris-Morini, P. Crozat, E. Cassan, J.-M. Fedeli, S. Brision, J.F. Damlencourt, V. Maxxochi, D. van Thourhout and J. Brouchaert, "European HELIOS Project: Silicon Photonic Photodetector Integration", **6th IEEE Int. Conf. on Group IV Photonics** (IEEE, San Francisco, CA, Sept., 2009), pp. 10-12.

[14] S. Fist, **The Informatics Handbook: a Guide to Multimedia Communications and Broadcasting**, London, UK: Springer, 1996.

[15] J.S. Huang and Y.H. Jan, "A New Kinetics Defect Diffusion Model and the Critical Current Density of Semiconductor Laser Degradation", **Appl. Phys. Res.**, Vol. 8, No. 4, 2016, pp. 11-19.

[16] M. Fukuda, **Optical Semiconductor Devices**, New York, NY: John Wiley & Sons, 1999.

[17] J.S. Huang, Y.H. Jan, D. Ren, Y. Hsu, P. Sung and E. Chou, "Defect Diffusion Model of InGaAs/InP Semiconductor Laser Degradation", **Appl. Phys. Res.**, Vol. 8, No. 1, 2016, pp. 149-157.

[18] J.S. Huang, Y.H. Jan, J. Chang, Y. Hsu, D. Ren and E. Chou, "Swift Reliability Test Methodology of 100G High-Speed, Energy-Efficient Electro-Absorption Modulated Lasers (EML) for Green Datacenter Networks", **Studies Eng. Tech.**, Vol. 3, No. 1, 2016, pp. 74-80.

[19] J.S. Huang, "Design-in Reliability for Modern Wavelength-Division Multiplex (WDM) Distributed Feedback (DFB) InP Lasers", **Appl. Phys. Res.**, Vol. 4, No. 2, 2012, pp. 15-28.

[20] J.S. Huang, A.S. Oates, Y.S. Obeng and W.L. Brown, "Asymmetrical Critical Current Density and Its Influence on Electromigration of Two-Level W-Plug Interconnection", **J. Electrochem. Soc**., Vol. 147, No. 10, 2000, pp. 3840-3844.

[21] J.S. Huang, T.L. Shofner and J. Zhao, "Direct Observation of Void Morphology in Step-Like Electromigration Resistance Behavior and Its Correlation with Critical Current Density", **J. Appl. Phys**., Vol. 89, No. 4, 2001, pp. 2130-2133.

[22] J.S. Huang, T. Tguyen, W. Hsin, I. Aeby, R. Ceballo and J. Krogen, "Reliability of Etched-Mesa Buried Heterostructure Semiconductor Lasers", **IEEE Tran. Device Mater. Reliab**., Vol. 5, No. 4, 2005, pp.665-674.

[23] J.S. Huang and A.S. Oates, "Monte-Carlo Simulation of Electromigration Failure Distribution of Submicron Contacts and Vias: a New Extrapolation Methodology for Reliability Estimate", **Proc. International Interconnect Technology Conference (IITC)**, 2000, pp. 208-210.

[24] I.A. Blech, "Electromigration in Thin Aluminum Films on Titanium Nitride", **J. Appl. Phys**., Vol. 47, 1976, pp. 1203-1208.

[25] I.A. Blech and C. Herring, "Stress Generation by Electromigration", **Appl. Phys. Lett**., Vol. 29, 1976, pp. 131-133.

[26] C.V. Thompson and J.R. Lloyd, "Electromigration and IC Interconnects", **MRS Bulletin**, 1993, pp. 19-25.

[27] J. Proost, K. Maex, and L. Delaey, "Electromigration-Induced Drift in Damascene and Plasma-Etched Al(Cu). II. Mass Transport Mechanisms in Bamboo Interconnects," **J. Appl. Phys**., Vol. 87, 2000, pp. 99–109.

[28] K.L. Lee, C.K. Hu and K.N. Tu, "In-Situ Scanning Electron Microscope Comparison Studies on Electromigration of Cu and Cu(Sn) Alloys for Advanced Chip Interconnects", **J. Appl. Phys**., Vol. 78, 1995, pp. 4428-4437

[29] A.S. Oates, "Electromigration Failure of Contacts and Vias in Sub-Micron Integrated Circuit Metallizations", **Microelectron. Reliab**., Vol. 36, No. 7/8, 1996, pp. 925-953.

[30] A.S. Oates and M.H. Lin, "Electromigration Failure Distributions of Cu/low-k Dual-Damascene Vias: Impact of the Citical Current Density and a New Reliability Extrapolation Methodology", **IEEE Trans. Dev. Mater. Reliab**., Vol. 9, No. 2, 2009, pp. 244-254.

[31] J.S. Huang, X.J. Deng, P.H. Yih, T.L. Shofner, Y.S. Obeng and C. Darling, "Effect of Silicon Nitride Capping Layer on Via Electromigration and Failure Criterion Methodology in Multilevel Interconnection", **Thin Solid Films**, Vol. 397, 2001, pp. 186-193.